Submitted to the
The 2007 Europhysics Conference on High Energy Physics
19-25 July 2007, Manchester, England

Abstract:
ZEUS-prel-07-013

Session: Strong Interactions

Jet substructure in neutral-current deep inelastic ep scattering at high Q^2 with HERA II

ZEUS Collaboration

Abstract

Jet substructure for jets produced in the deep inelastic ep scattering regime has been studied for exchanged boson virtualities $Q^2 > 125$ GeV^2 with the ZEUS detector using 368 pb^{-1} of integrated luminosity from the HERA II running period. Jets were identified in the laboratory frame using the k_T cluster algorithm in the longitudinally invariant inclusive mode. The substructure of jets has been investigated in terms of the jet shape and used to highlight differences between quark- and gluon-initiated jets. Leading-logarithm parton-shower Monte Carlo models and next-to-leading-order QCD calculations are compared to the data and describe the measurements well.

1 Introduction

Jet production in ep collisions provides a fruitful testing ground of perturbative QCD (pQCD). Measurements of differential cross sections for jet production [1, 2] have allowed detailed studies of parton dynamics, tests of the proton and photon parton distribution functions (PDFs) as well as precise determinations of the strong coupling constant, α_s. Most of these measurements refer to the production of jets irrespective of their partonic origin – quarks or gluons – and, therefore, have only provided general tests of the partonic structure of the short-distance process and of combinations of the proton and/or photon PDFs.

The identification of quark- and gluon-initiated jets allows more stringent tests of the QCD predictions. Such measurements of the production of jets containing a heavy quark have been made by means of tagging specific decay channels [3]. In a recent study [4], quark- and gluon-initiated jets were identified on a statistical basis by utilising their internal structure: in the photoproduction regime, it was shown that "broad" ("narrow") jets had a dynamic behaviour in terms of differential cross sections as expected from gluon- (quark-) initiated jets and a sample of inclusive jets in neutral current (NC) deep inelastic scattering (DIS) was consistent with being dominated by quark-initiated jets.

Another aspect of QCD, namely gluon emission from a primary quark, can also be investigated by means of the internal structure of jets; such a study gives insight into the transition between a parton produced in a hard process and the experimentally observable jet of hadrons. In a previous study [5], the pattern of QCD radiation was investigated by means of the subjet topology, yielding a very stringent test of pQCD calculations. This paper presents a deeper study of the parton content of the final state in NC DIS processes by means of the jet shape. Jet production in NC DIS up to leading order (LO) in α_s proceeds as in the quark-parton model (QPM, $V^*q \to q$, where $V = \gamma$ or Z^0) or via the boson-gluon fusion (BGF, $V^*g \to q\bar{q}$) and QCD-Compton (QCDC, $V^*q \to qg$) processes. Therefore, different types of jet samples would be dominated by different parton content in the final state. This fact was exploited in this analysis to highlight differences between quark- and gluon-initiated jets.

2 Theoretical expectations

The internal structure of a jet depends mainly on the type of primary parton – quark or gluon – from which it originated and to a lesser extent on the particular hard scattering process. At sufficiently high jet transverse energy, where the influence of fragmentation effects becomes negligible, the internal structure of a jet is calculable in pQCD. Such calculations predict that gluon-initiated jets are broader than quark-initiated jets due to the larger colour charge of the gluon.

In zeroth-order pQCD, a jet consists of only one parton and the jets have no substructure. The first non-trivial contribution to the jet substructure is given by $\mathcal{O}(\alpha_s)$ processes in which, e.g., a quark radiates a gluon at a small angle; these are proportional to the rate of parton emission and to α_s.

2.1 Jet-shape definition

The jet shape [6] can be used to study the internal structure of the jets. The k_T cluster algorithm [7] was used in the longitudinally invariant inclusive mode [8] to define jets in the hadronic final state in the laboratory frame. The integrated jet shape, $\psi(r)$, is defined using only those particles belonging to the jet as the fraction of the jet transverse energy that lies inside a circle in the $\eta - \phi$ plane of radius r concentric with the jet axis:

$$\psi(r) = \frac{E_T(r)}{E_T^{\text{jet}}},$$

where $E_T(r)$ is the transverse energy within the given circle of radius r. The mean integrated jet shape, $\langle\psi(r)\rangle$, is defined as the averaged fraction of the jet transverse energy inside the circle:

$$\langle\psi(r)\rangle = \frac{1}{N_{\text{jets}}} \sum_{\text{jets}} \frac{E_T(r)}{E_T^{\text{jet}}},$$

where N_{jets} is the total number of jets in the sample.

The integrated jet shape is calculated at LO in pQCD as the fraction of the jet transverse energy, due to parton emission, that lies between circles of radii r and $R = 1$:

$$\langle 1 - \psi(r)\rangle = \frac{\int_r^R dE_T \ (E_T/E_T^{\text{jet}}) \ [d\sigma(ep \to 2 \text{ partons})/dE_T]}{\sigma_{\text{jet}}(E_T^{\text{jet}})},$$

where $\sigma_{\text{jet}}(E_T^{\text{jet}})$ is the cross section for inclusive-jet production. In the next-to-leading-order (NLO) QCD predictions of the integrated jet shape, the numerator in the above formula is calculated to $\mathcal{O}(\alpha\alpha_s^2)$ and the denominator to $\mathcal{O}(\alpha\alpha_s)$.

3 Experimental set-up

A detailed description of the ZEUS detector can be found elsewhere [9,10]. A brief outline of the components most relevant for this analysis is given below.

Charged particles were tracked in the central tracking detector (CTD) [11], which operated in a magnetic field of 1.43 T provided by a thin superconducting solenoid. The high-resolution uranium–scintillator calorimeter (CAL) [12] covered 99.7% of the total solid angle and consisted of three parts: the forward (FCAL), the barrel (BCAL) and the rear (RCAL) calorimeters. Each part was subdivided transversely into towers and longitudinally into one electromagnetic section (EMC) and either one (in RCAL) or two (in BCAL and FCAL) hadronic sections (HAC). The smallest subdivision of the calorimeter was called a cell. The luminosity was measured using the Bethe-Heitler reaction $ep \to e\gamma p$ by the luminosity detector which consisted of two independent systems [13]

4 Data selection and jet search

The data used in this analysis were collected during the 2004-2007 running period and correspond to an integrated luminosity of 368 pb^{-1}.

Various TLT trigger slots, requiring either the identification of an electron[1] candidate or a jet in the CAL were used to select online the NC DIS sample. In the offline selection, a reconstructed event vertex consistent with the nominal interaction position was required and cuts based on the tracking information were applied to reduce the contribution from beam-induced interactions and cosmic-ray events. The main steps of the selection are briefly explained below.

Events from NC DIS interactions were selected offline using similar criteria to those reported in a previous publication [4]. The scattered-electron candidate was identified using the pattern of energy deposits in the CAL [14]. The energy, E'_e, and polar angle, θ_e, of the electron candidate were also determined from the CAL measurements. The double-angle method [15] was used to reconstruct Q^2.

An electron candidate of energy $E'_e > 10$ GeV was required to ensure a high and well understood electron-finding efficiency and to suppress background from photoproduction. The inelasticity variable as reconstructed from the electron was required to be below 0.95; this condition removed events in which fake electron candidates from photoproduction background were found in the FCAL. The requirements $38 < (E - p_Z) < 65$ GeV, to remove events with large initial-state radiation and to reduce further the photoproduction background, and $p_T^{\rm miss}/\sqrt{E_T^{\rm tot}} < 3\ \sqrt{\rm GeV}$, to remove cosmic rays and beam-related background, were applied. The kinematic range was restricted to $Q^2 > 125$ GeV^2.

[1] Here and in the following, the term "electron" denotes generically both the electron (e^-) and the positron (e^+).

4.1 Jet search

The k_T cluster algorithm was used in the longitudinally invariant inclusive mode to reconstruct jets in the hadronic final state from the energy deposits in the CAL cells. The jet algorithm was applied after excluding those cells associated with the scattered-electron candidate. The jet search was performed in the $\eta-\phi$ plane of the laboratory frame. The jet variables were defined according to the Snowmass convention [16]. The jets reconstructed from the CAL cell energies are called calorimetric jets and the variables associated with them are denoted by $E_{T,\mathrm{cal}}^{\mathrm{jet}}$, $\eta_{\mathrm{cal}}^{\mathrm{jet}}$ and $\varphi_{\mathrm{cal}}^{\mathrm{jet}}$. A total of 865 714 events with at least one jet satisfying $E_{T,\mathrm{cal}}^{\mathrm{jet}} > 9$ GeV and $-1 < \eta_{\mathrm{cal}}^{\mathrm{jet}} < 2.5$ were selected.

4.2 Jet samples

After jet-energy corrections (see Section 6.1), events with jets of $E_T^{\mathrm{jet}} > 14$ GeV were retained. Several jet samples were selected:

- **inclusive-jet sample:** all jets in each event;
- **one-jet sample:** events with exclusively one jet;
- **lowest-E_T^{jet}-$D = 2.0$ sample:** events with exclusively two-jets and a distance in the $\eta - \phi$ plane between the two jets of $D \leq 2.0$. The jet with lowest E_T^{jet} was studied;
- **lowest-E_T^{jet}-$D = 2.5$ sample:** events with exclusively two-jets and a distance in the $\eta - \phi$ plane between the two jets of $D \leq 2.5$. The jet with lowest E_T^{jet} was studied.

Measurements of the mean integrated jet shape were made for these samples with jets of $E_T^{\mathrm{jet}} > 14$ GeV and also restricting the jet transverse energy to the range $14 < E_T^{\mathrm{jet}} < 17$ GeV.

5 QCD calculations

5.1 Leading-logarithm parton-shower Monte Carlo models

Neutral current DIS events including radiative effects were simulated using the Heracles 4.6.1 [17] program with the Djangoh 1.1 [18] interface to the hadronisation programs. Heracles includes corrections for initial- and final-state radiation, vertex and propagator terms, and two-boson exchange. The QCD cascade is simulated using the colour-dipole model (CDM) [19] including the LO QCD diagrams as implemented in Ariadne 4.08 [20] and, as a systematic check of the final results, with the MEPS model of Lepto 6.5 [21]. Both MC programs use the Lund string model [22], as implemented in JETSET [23, 24], for the hadronisation. The CTEQ5D [25] proton PDFs were used for these simulations.

These MC samples were used to correct the data to the hadron level, defined as those hadrons with lifetime $\tau \geq 10$ ps. For this purpose, the generated events were passed through the ZEUS detector- and trigger-simulation programs based on GEANT 3.13 [26]. They were reconstructed and analysed by the same program chain as the data. The jet search was performed using the energy measured in the CAL cells in the same way as for the data. The same jet algorithm was also applied to the final-state particles and to the partons available after the parton shower; the jets found in this way are referred to as hadronic and partonic jets, respectively.

Electroweak-radiative, hadronisation and Z^0-exchange effects are not at present included in the NLO QCD programs described in Section 5.2. Therefore, samples of MC events were generated without electroweak-radiative effects so that the data could be corrected for these effects. These factors differ from unity by less than 5%. These MC samples were also used to make the predictions that are compared to the data. Additional samples of MC events without Z^0-exchange effects were generated to correct the NLO QCD calculations for such effects and for hadronisation.

5.2 NLO QCD calculations

The NLO QCD calculations of the mean integrated jet shapes in DIS are based on the programs DISENT [27] and NLOJET++ [28]. The calculations use a generalised version of the subtraction method [29] and are performed in the massless $\overline{\text{MS}}$ renormalisation and factorisation schemes. The number of flavours was set to five; the renormalisation (μ_R) and factorisation (μ_F) scales were both set to $\mu_R = \mu_F = Q$; α_s was set to 0.118. The CTEQ6 [30] parameterisations of the proton PDFs were used. The calculations obtained with DISENT were used for comparison to the inclusive and one-jet measurements, whereas the predictions from NLOJET++ were compared to the two-jet measurements.

Since the measurements refer to jets of hadrons, whereas the QCD calculations refer to partons, the predictions were corrected to the hadron level using the MC samples described in Section 5.1. The multiplicative correction factor, C_{had}, defined as $\langle\psi(r)\rangle_{\text{had}}/\langle\psi(r)\rangle_{\text{par}}$, where $\langle\psi(r)\rangle_{\text{par (had)}}$ is the mean integrated jet shape before (after) the hadronisation process, was estimated with the CDM model. The correction factors applied to the NLO calculations, which include hadronisation and Z^0 effects, are below 10% for $r \geq 0.4$. The procedure for applying hadronisation corrections to the NLO QCD calculations was verified by checking that the MC predictions for the integrated jet shape at the parton level reproduced the NLO QCD calculations. The agreement is very good for $r > 0.1$

after adjusting the contributions of the different subprocesses (QPM, BGF and QCDC) in the MC to reproduce the mean integrated jet shape of the NLO calculations.

6 Corrections and systematic uncertainties

6.1 Jet energy corrections

The comparison of the reconstructed jet variables for the hadronic and the calorimetric jets in simulated events showed that no correction was needed for $\eta^{\rm jet}$ and $\phi^{\rm jet}$ ($\eta^{\rm jet} \simeq \eta^{\rm jet}_{\rm cal}$ and $\phi^{\rm jet} \simeq \varphi^{\rm jet}_{\rm cal}$). However, the transverse energy of the calorimetric jet was an underestimate of the corresponding hadronic jet energy by an average of $\sim 15\%$, with an r.m.s. of $\sim 10\%$. This underestimation was mainly due to the energy lost by the particles in the inactive material in front of the CAL. The transverse-energy corrections to calorimetric jets, as a function of $\eta^{\rm jet}_{\rm cal}$ and $E^{\rm jet}_{T,\rm cal}$ and averaged over $\varphi^{\rm jet}_{\rm cal}$, were determined using the MC-generated events [2]. After these corrections to the jet transverse energy, events with at least one jet satisfying $E_T^{\rm jet} > 14$ GeV and $-1 < \eta^{\rm jet} < 2.5$ were retained. Four samples of jets were studied, as explained in Section 4.2.

6.2 Acceptance corrections and experimental uncertainties

Using the selected data samples of inclusive jets, one jet and two jets with $E_T^{\rm jet} > 14$ GeV and $-1 < \eta^{\rm jet} < 2.5$, in the kinematic region defined by $Q^2 > 125$ GeV^2, the mean integrated jet shape was reconstructed using the CAL cells and corrected to the hadron level by MC techniques. The corrected values were determined bin-by-bin using the MC samples. For this approach to be valid, the distributions of the uncorrected integrated jet shape in the data must be well described by the MC simulations at the detector level. To obtain the best description of the uncorrected jet shape in the data by the MC simulations, the contributions of the different subprocesses (QPM, BGF and QCDC) were reweighted so as to reproduce the mean integrated jet shape in the data. This procedure was applied to the simulations of CDM and MEPS. The CDM MC provides a good description of all samples. The MEPS MC fails to describe the two-jet sample. The correction factors to the data were evaluated using this tuned version of CDM; they differed from unity by $\sim 15\%$ for $r = 0.3$ and by less than 10% for $r \geq 0.5$.

The sources contributing to the systematic uncertainties of the measurements considered are:

- the effect of the treatment of the parton shower was estimated by using the MEPS model to evaluate the correction factors;

- the effect of the uncertainty of $\pm 3\%$ in the absolute energy scale of the jets was applied to the simulated events.

These uncertainties were added in quadrature to the statistical uncertainty of the data and are shown as error bars in the figures. Since the MEPS MC does not describe well the two-jet sample, the contribution to the experimental uncertainty from this source is dominant in that case.

7 Results

The measured mean integrated jet shape as a function of r, $\langle\psi(r)\rangle$, for $E_T^{\rm jet} > 14$ GeV is shown in Fig. 1a for the inclusive-jet sample and in Fig. 1b for the one-jet sample. The predictions of the QCD-inspired Monte Carlo model of CDM give a good description of the data, whereas the MEPS calculations predict jets broader than the data.

The measurements for the inclusive-jet and one-jet samples are very similar, which demonstrates that the inclusive-jet sample is dominated by one-jet events. The one-jet events would come mainly from the QPM processes, namely it is a quark-enriched sample. A sample with two jets, whose events would come from the BGF and QCDC processes, would have a higher gluon content in the final state. Jets from gluon radiation are expected to be closer to the primary parton and to have a lower $E_T^{\rm jet}$ than the primary parton. Therefore, the lowest-$E_T^{\rm jet}$ jet from a sample of two-jet events for which the two jets are close in $\eta - \phi$ is expected to be a gluon and, as predicted by QCD, broader than quark-initiated jets. Figs 1c and 1d show the mean integrated jet shape for such jets with a distance $D \leq 2.0$ and $D \leq 2.5$ between the two jets, respectively, compared with the measurement for the one-jet sample; it is observed that the lowest-$E_T^{\rm jet}$ jets are broader than those in the one-jet sample. This observation is consistent with a higher gluon content in two-jet events. The predictions of CDM give a good description of the data; in particular, the Monte Carlo reproduces the difference in jet shape between the two samples.

The mean integrated jet shape increases as $E_T^{\rm jet}$ increases, as shown in previous studies. To remove this dependency only jets with $14 < E_T^{\rm jet} < 17$ GeV were considered. Figure 2 shows the mean integrated jet shape for all the samples studied in this restricted range in $E_T^{\rm jet}$. The same conclusions as in the whole $E_T^{\rm jet}$ range are drawn. The predictions of CDM give jets that are slightly broader than in the data.

In Figs 3 and 4, the NLO calculations, corrected for hadronisation and Z^0 effects, are compared to the data. The predictions give a very good description of the data in all cases; in particular, the NLO predictions reproduce the difference in jet shape between the one-jet and two-jet samples.

8 Summary and conclusions

Jet substructure has been studied using 368 pb^{-1} of integrated luminosity from HERA II data. The mean integrated jet shape of jets in a sample of one-jet events has been compared to that of jets in a two-jet sample with jets that are close in the $\eta - \phi$ plane. The results are compatible with the two-jet sample being enriched in gluon-initiated jets. The NLO calculations give a very good description of the data; in particular, the NLO predictions reproduce the difference in jet shape between the one-jet and two-jet samples.

The observed differences in jet shape between the one-jet and two-jet samples will be in the future exploited to disentangle the quark and gluon contributions to the final state.

References

[1] ZEUS Coll., J. Breitweg et al., Phys. Lett. **B 443**, 394 (1998);
ZEUS Coll., J. Breitweg et al., Phys. Lett. **B 507**, 70 (2001);
ZEUS Coll., S. Chekanov et al., Eur. Phys. J. **C 23**, 13 (2002);
ZEUS Coll., S. Chekanov et al., Phys. Lett. **B 547**, 164 (2002);
ZEUS Coll., S. Chekanov et al., Phys. Lett. **B 560**, 7 (2003);
ZEUS Coll., S. Chekanov et al., Eur. Phys. J. **C 31**, 149 (2003).

[2] ZEUS Coll., S. Chekanov et al., Phys. Lett. **B 531**, 9 (2002);
ZEUS Coll., S. Chekanov et al., Eur. Phys. J. **C 23**, 615 (2002);
ZEUS Coll., S. Chekanov et al., Phys. Lett. **B 558**, 41 (2003).

[3] ZEUS Coll., S. Chekanov et al., Phys. Lett. **B 565**, 87 (2003);
ZEUS Coll., S. Chekanov et al., Phys. Rev. **D 70**, 012008 (2004).

[4] ZEUS Coll., S. Chekanov et al., Nucl. Phys. **B 700**, 3 (2004).

[5] ZEUS Coll., *Subjet distributions in inclusive-jet production in deep inelastic scattering at HERA*. Abstract 56, The 2007 Europhysics Conference on High Energy Physics, 19-25 July 2007, Manchester, England, 2007.

[6] S.D. Ellis, Z. Kunszt and D.E. Soper, Phys. Rev. Lett. **69**, 3615 (1992).

[7] S. Catani et al., Nucl. Phys. **B 406**, 187 (1993).

[8] S.D. Ellis and D.E. Soper, Phys. Rev. **D 48**, 3160 (1993).

[9] ZEUS Coll., M. Derrick et al., Phys. Lett. **B 293**, 465 (1992).

[10] ZEUS Coll., U. Holm (ed.), *The ZEUS Detector*. Status Report (unpublished), DESY (1993), available on `http://www-zeus.desy.de/bluebook/bluebook.html`.

[11] N. Harnew et al., Nucl. Inst. Meth. **A 279**, 290 (1989);
B. Foster et al., Nucl. Phys. Proc. Suppl. **B 32**, 181 (1993);
B. Foster et al., Nucl. Inst. Meth. **A 338**, 254 (1994).

[12] M. Derrick et al., Nucl. Inst. Meth. **A 309**, 77 (1991);
A. Andresen et al., Nucl. Inst. Meth. **A 309**, 101 (1991);
A. Caldwell et al., Nucl. Inst. Meth. **A 321**, 356 (1992);
A. Bernstein et al., Nucl. Inst. Meth. **A 336**, 23 (1993).

[13] J. Andruszków et al., Preprint DESY-92-066, DESY, 1992;
ZEUS Coll., M. Derrick et al., Z. Phys. **C 63**, 391 (1994);
J. Andruszków et al., Acta Phys. Pol. **B 32**, 2025 (2001);
M. Helbich et al., Nucl. Inst. Meth. **A 565**, 572 (2006).

[14] H. Abramowicz, A. Caldwell and R. Sinkus, Nucl. Inst. Meth. **A 365**, 508 (1995); R. Sinkus and T. Voss, Nucl. Inst. Meth. **A 391**, 360 (1997).

[15] S. Bentvelsen, J. Engelen and P. Kooijman, *Proc. of the Workshop on Physics at HERA*, W. Buchmüller and G. Ingelman (eds.), Vol. 1, p. 23. Hamburg, Germany, DESY (1992);
K.C. Höger, ibid., p. 43.

[16] J.E. Huth et al., *Research Directions for the Decade. Proc. of Summer Study on High Energy Physics, 1990*, E.L. Berger (ed.), p. 134. World Scientific (1992). Also in preprint FERMILAB-CONF-90-249-E.

[17] A. Kwiatkowski, H. Spiesberger and H.-J. Möhring, Comp. Phys. Comm. **69**, 155 (1992);
H. Spiesberger, *An Event Generator for ep Interactions at HERA Including Radiative Processes (Version 4.6)*, 1996, available on
`http://www.desy.de/~hspiesb/heracles.html`.

[18] K. Charchuła, G.A. Schuler and H. Spiesberger, Comp. Phys. Comm. **81**, 381 (1994);
H. Spiesberger, HERACLES *and* DJANGOH*: Event Generation for ep Interactions at HERA Including Radiative Processes*, 1998, available on
`http://wwwthep.physik.uni-mainz.de/~hspiesb/djangoh/djangoh.html`.

[19] Y. Azimov et al., Phys. Lett. **B 165**, 147 (1985);
G. Gustafson, Phys. Lett. **B 175**, 453 (1986);
G. Gustafson and U. Pettersson, Nucl. Phys. **B 306**, 746 (1988);
B. Andersson et al., Z. Phys. **C 43**, 625 (1989).

[20] L. Lönnblad, Comp. Phys. Comm. **71**, 15 (1992);
L. Lönnblad, Z. Phys. **C 65**, 285 (1995).

[21] G. Ingelman, A. Edin and J. Rathsman, Comp. Phys. Comm. **101**, 108 (1997).

[22] B. Andersson et al., Phys. Rep. **97**, 31 (1983).

[23] T. Sjöstrand, Comp. Phys. Comm. **82**, 74 (1994);
T. Sjöstrand et al., Comp. Phys. Comm. **135**, 238 (2001).

[24] T. Sjöstrand, Comp. Phys. Comm. **39**, 347 (1986);
T. Sjöstrand and M. Bengtsson, Comp. Phys. Comm. **43**, 367 (1987).

[25] H.L. Lai et al., Eur. Phys. J. **C 12**, 375 (2000).

[26] R. Brun et al., GEANT3, Technical Report CERN-DD/EE/84-1, CERN, 1987.

[27] S. Catani and M.H. Seymour, Nucl. Phys. **B 485**, 291 (1997). Erratum in Nucl. Phys. B 510 (1998) 503.

[28] Z. Nagy and Z. Trocsanyi, Phys. Rev. Lett. **87**, 082001 (2001).

[29] R.K. Ellis, D.A. Ross and A.E. Terrano, Nucl. Phys. **B 178**, 421 (1981).

[30] J. Pumplin et al., JHEP **0207**, 012 (2002);
D. Stump et al., JHEP **0310**, 046 (2003).

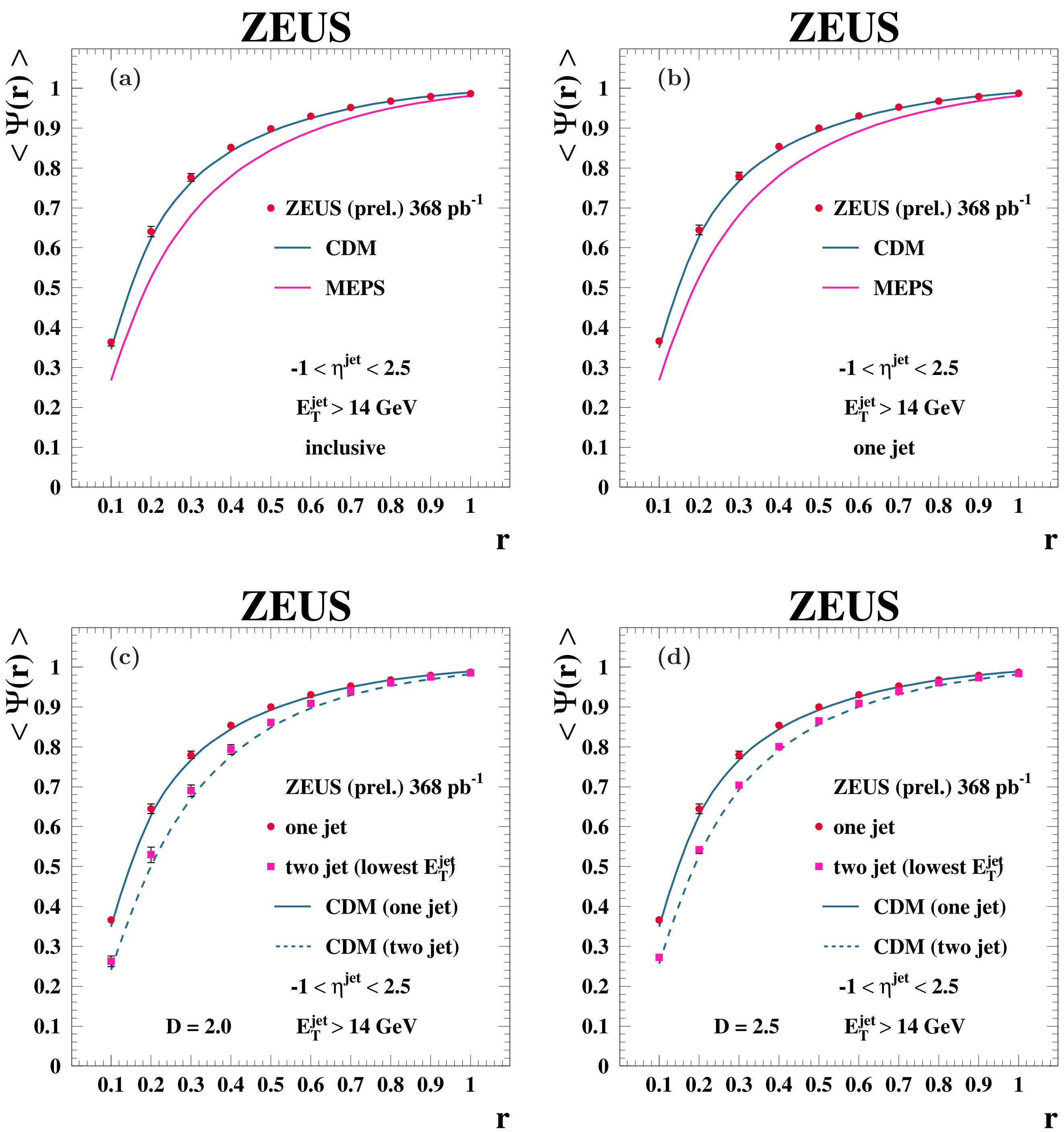

Figure 1: *Measured mean integrated jet shape as a function of r for jets with $-1 < \eta^{\rm jet} < 2.5$ and $E_T^{\rm jet} > 14$ GeV in the kinematic range given by $Q^2 > 125$ GeV^2 for the (a) inclusive-jet (dots), (b) one-jet (dots), (c) one-jet (dots) and two-jet (lowest-$E_T^{\rm jet}$, $D = 2.0$) (squares) and (d) one-jet (dots) and two-jet (lowest-$E_T^{\rm jet}$, $D = 2.5$) (squares) samples. The error bars represent the experimental uncertainties. For comparison, the predictions of the CDM (blue lines) and MEPS (pink lines) models are included.*

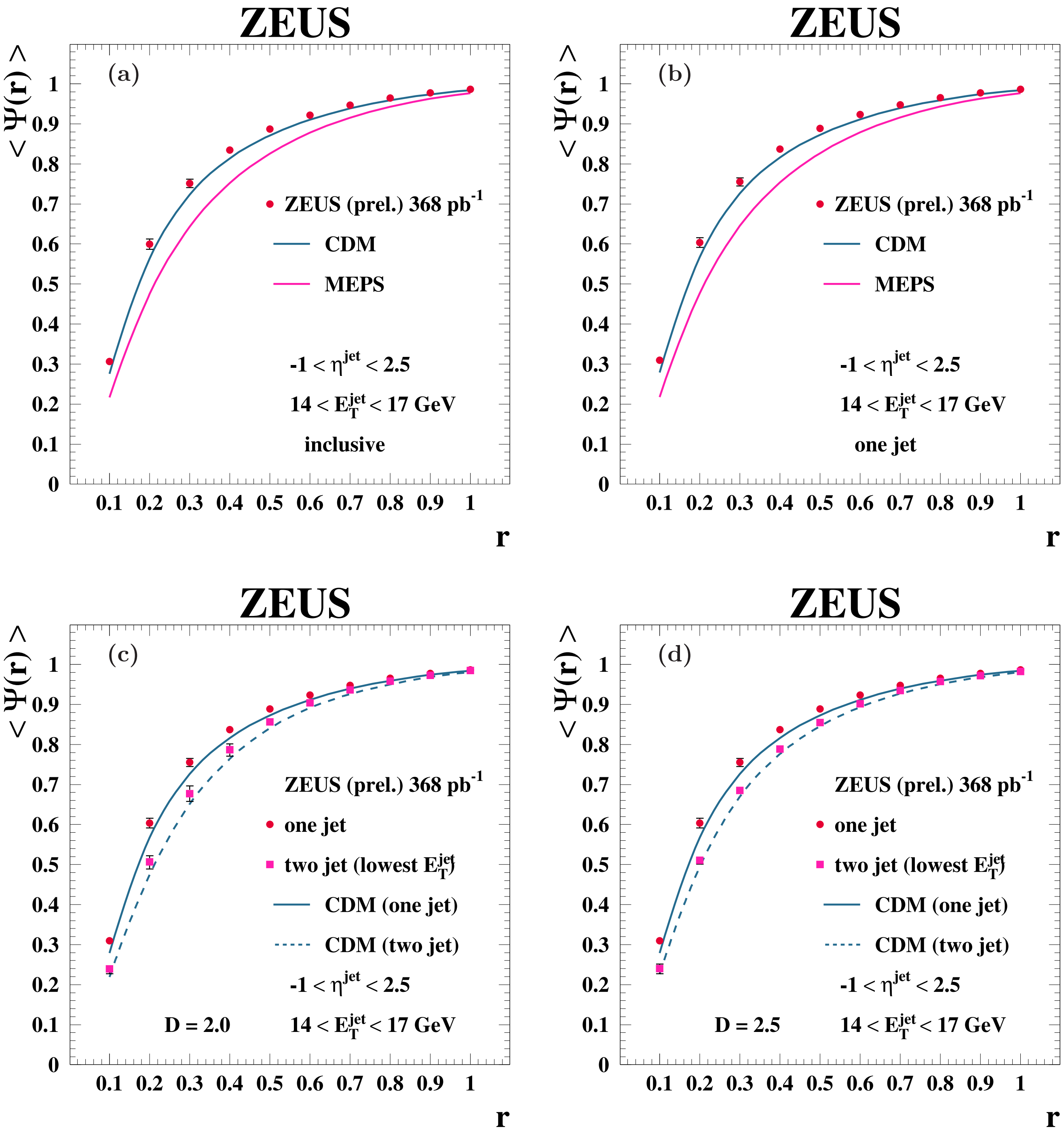

Figure 2: *Measured mean integrated jet shape as a function of r for jets with $-1 < \eta^{\rm jet} < 2.5$ and $14 < E_T^{\rm jet} < 17$ GeV in the kinematic range given by $Q^2 > 125$ GeV^2 for the (a) inclusive-jet (dots), (b) one-jet (dots), (c) one-jet (dots) and two-jet (lowest-$E_T^{\rm jet}$, $D = 2.0$) (squares) and (d) one-jet (dots) and two-jet (lowest-$E_T^{\rm jet}$, $D = 2.5$) (squares) samples. The error bars represent the experimental uncertainties. For comparison, the predictions of the CDM (blue lines) and MEPS (pink lines) models are included.*

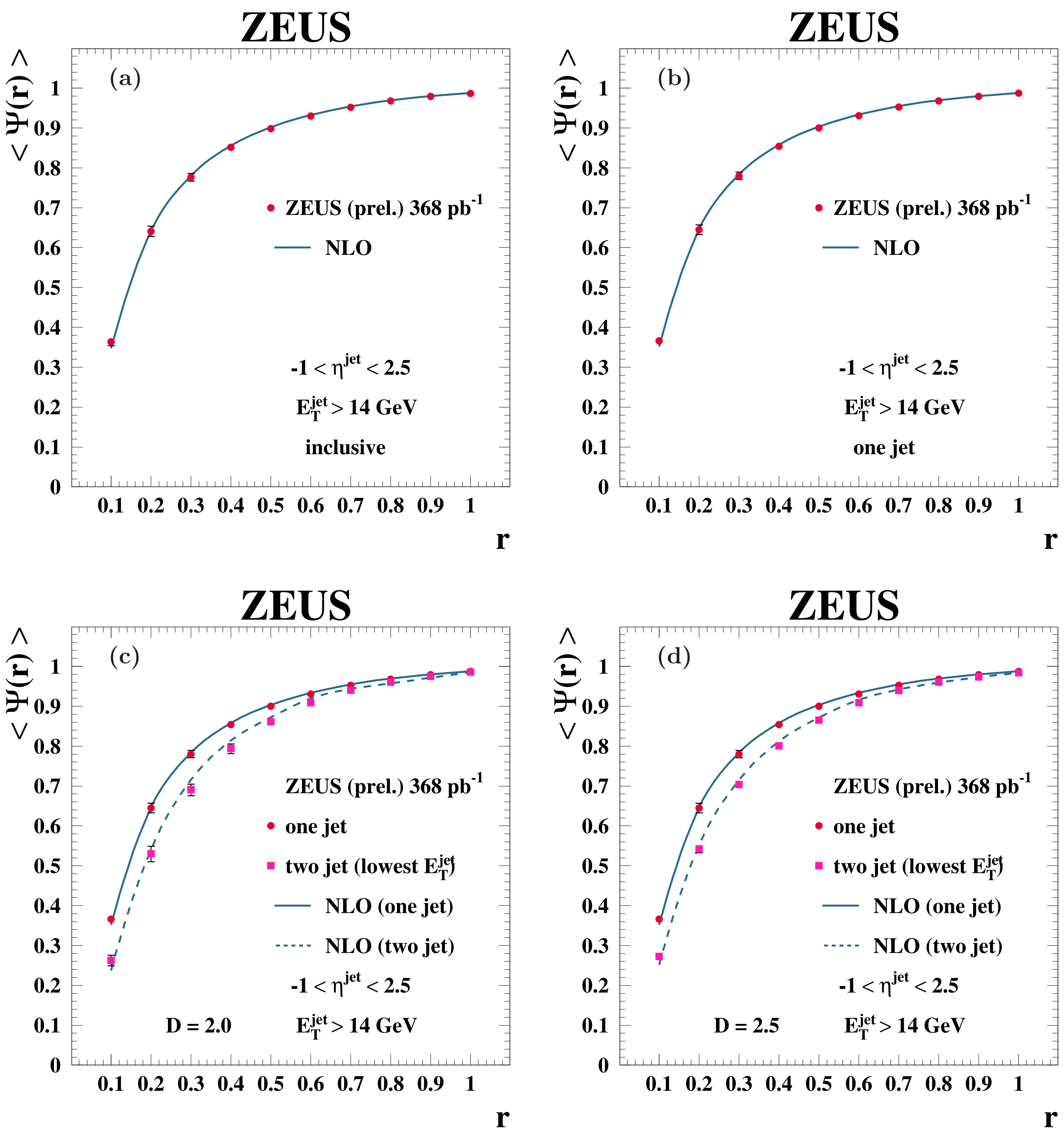

Figure 3: *Measured mean integrated jet shape as a function of r for jets with $-1 < \eta^{\rm jet} < 2.5$ and $E_T^{\rm jet} > 14$ GeV in the kinematic range given by $Q^2 > 125$ GeV^2 for the (a) inclusive-jet (dots), (b) one-jet (dots), (c) one-jet (dots) and two-jet (lowest-$E_T^{\rm jet}$, $D = 2.0$) (squares) and (d) one-jet (dots) and two-jet (lowest-$E_T^{\rm jet}$, $D = 2.5$) (squares) samples. The error bars represent the experimental uncertainties. For comparison, the predictions of the NLO calculations (blue lines) are included.*

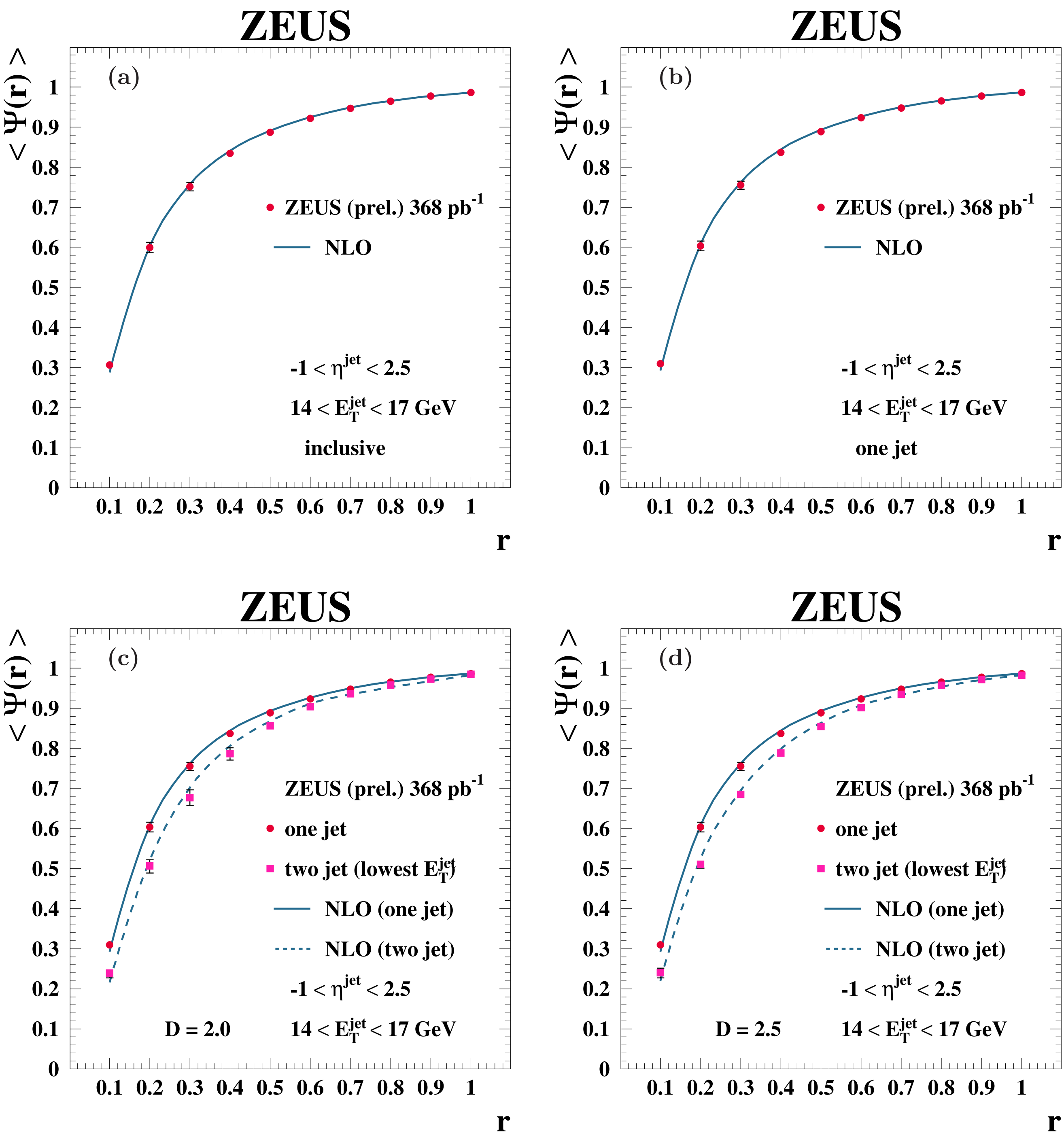

Figure 4: *Measured mean integrated jet shape as a function of r for jets with $-1 < \eta^{\rm jet} < 2.5$ and $14 < E_T^{\rm jet} < 17$ GeV in the kinematic range given by $Q^2 > 125$ GeV^2 for the (a) inclusive-jet (dots), (b) one-jet (dots), (c) one-jet (dots) and two-jet (lowest-$E_T^{\rm jet}$, $D = 2.0$) (squares) and (d) one-jet (dots) and two-jet (lowest-$E_T^{\rm jet}$, $D = 2.5$) (squares) samples. The error bars represent the experimental uncertainties. For comparison, the predictions of the NLO calculations (blue lines) are included.*